Impact of the cap layer on the electronic structures and optical properties of self-assembled InAs/GaAs quantum dots

Hai-Bin Wu, S. J. Xu,* and Jian Wang
Department of Physics, The University of Hong Kong, Pokfulam Road, Hong Kong, China
(Received 17 December 2005; revised manuscript received 7 September 2006; published 21 November 2006)

Cap layer impact on the electronic structures and optical properties of self-assembled InAs/GaAs quantum dots is theoretically studied within the framework of Burt and Foreman's eight-band effective-mass Hamiltonian. A numerically stable finite difference scheme for this nonsymmetrized Hamiltonian and an efficient implementation of Jacobi-Davidson eigensolver for the resulting matrix are proposed. Our theoretical results show that as the cap layer thickness increases, the photoluminescence (PL) peak position exhibits a monotonous blueshift and the PL intensity enhances. These results are accounted for by the strain modified band edges and the space separation of electron and heavy-hole wave functions in the growth direction. Dot shape and size effects are also discussed. Our calculations are in good agreement with recent experimental findings.

DOI: 10.1103/PhysRevB.74.205329 PACS number(s): 73.21.La, 78.67.Hc, 78.20.Bh

I. INTRODUCTION

Self-assembled InAs/GaAs QDs have received great attention during the past decade.[1] They not only provide ideal entities for studying 3D quantum confinement effects on carriers but also find their usage in optoelectronic semiconductor devices. When they are considered as candidates for laser diodes, one of the key issues is to achieve 1.3 μm or longer optical emission wavelengths. Several groups[2–9] have reported that a wide range of wavelength can be obtained if the environment around the InAs QDs is modified, such as the material compositions of the underlaying and cap layers, and the thickness of the cap layer.

Theoretically the InAs/GaAs pyramidal QDs have already been studied by several groups using the $\mathbf{k}\cdot\mathbf{p}$,[10–16] psuedopotential,[17–19] and tight-binding[20,21] methods. However, most of these works focus on the properties of the fully capped QDs and only a few concern the free-standing InAs QDs.[19,20] To our knowledge, detailed theoretical study on the GaAs cap layer influences is still lacking even though they are very important in determining the QDs' optical properties.

In this work, we theoretically investigate these influences on the electronic states and the photoluminescence (PL) properties of the self-assembled InAs/GaAs QDs. An eight-band $\mathbf{k}\cdot\mathbf{p}$ nonsymmetrized Hamiltonian[22] is used to solve the electronic states. The details of our theoretical model and numerical method are also presented. By varying the cap layer thickness in a wide range, we find that PL spectrum shows a large blueshift in energy and an increase in intensity.

II. THEORETICAL MODEL AND NUMERICAL METHOD

We consider a truncated pyramidal InAs/GaAs QD covered with a uniformly thick GaAs cap layer as shown in the inset of Fig. 1. Shape change and In/Ga interdiffusion during the deposition process are neglected. Furthermore we focus on the states confined in the QD and neglect the influences of the wetting layer and the surface states. The small piezoelectric effect[10] is also discarded here.

A. Hamiltonian

The kinetic part of the Hamiltonian is based on Burt's exact envelope function theory[23] and the specific form for the four-band effective-mass Hamiltonian without spin-orbit interaction is[22,24]

$$H_4 = \begin{bmatrix} H_{cc} & H_{cv} \\ H_{vc} & H_{vv} \end{bmatrix}, \tag{1}$$

with bases

$$|S\rangle, |X\rangle, |Y\rangle, |Z\rangle. \tag{2}$$

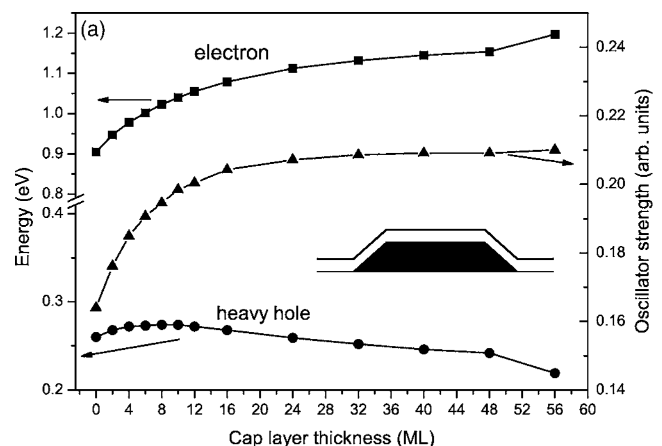

FIG. 1. Ground-state energies and oscillator strengths for the [100]/[010] polarized light as a function of cap layer thickness. The QD's width and height are 25.4 and 5.1 nm, respectively. Note that electron and hole energies are not on the same scale.

 ©2006 The American Physical Society

In Eq. (1),

$$H_{cc} = E_c + kA_ck, \tag{3}$$

$$A_c = \hbar^2/2m_c - 2P^2/3E_g - P^2/3(E_g + \Delta), \tag{4}$$

and

$$H_{cv} = [iPk_x \; iPk_y \; iPk_z],$$

$$H_{vc} = [-ik_xP \; -ik_yP \; -ik_zP]^T, \tag{5}$$

$$H_{vv} = \frac{\hbar^2}{2m_0}\begin{bmatrix} k_xAk_x + k_yBk_y + k_zBk_z & k_xC_1k_y - k_yC_2k_x & k_xC_1k_z - k_zC_2k_x \\ k_yC_1k_x - k_xC_2k_y & k_yAk_y + k_xBk_x + k_zBk_z & k_yC_1k_z - k_zC_2k_y \\ k_zC_1k_x - k_xC_2k_z & k_zC_1k_y - k_yC_2k_z & k_zAk_z + k_xBk_x + k_yBk_y \end{bmatrix}, \tag{6}$$

where

$$A = -\gamma_1 - 4\gamma_2, \quad B = -\gamma_1 + 2\gamma_2,$$

$$C_1 = \gamma_1 - 2\gamma_2 - 6\gamma_3, \quad C_2 = \gamma_1 - 2\gamma_2 + 1. \tag{7}$$

The modified Luttinger parameters γ_i are determined from the usual Luttinger parameters γ_i^L by

$$\gamma_1 = \gamma_1^L - E_p/3E_g,$$

$$\gamma_2 = \gamma_2^L - E_p/6E_g,$$

$$\gamma_3 = \gamma_3^L - E_p/6E_g. \tag{8}$$

To eliminate the physically spurious solutions of the Hamiltonian (1), we take Foreman's approach[22] by setting $A_c=0$ and adjusting P to fit conduction band effective mass m_c. As will be shown in Sec. II C, this approach can also greatly reduce the computational efforts.

The strain Hamiltonian in bases (2) is described by Bahder's model[25]

$$H_{\rm str} = \begin{bmatrix} a_c(e_{xx}+e_{yy}+e_{zz}) & -iP_0\sum_j e_{xj}k_j & -iP_0\sum_j e_{yj}k_j & -iP_0\sum_j e_{zj}k_j \\ i\sum_j k_je_{xj}P_0 & le_{xx}+m(e_{yy}+e_{zz}) & ne_{xy} & ne_{xz} \\ i\sum_j k_je_{yj}P_0 & ne_{xy} & le_{yy}+m(e_{xx}+e_{zz}) & ne_{yz} \\ i\sum_j k_je_{zj}P_0 & ne_{xz} & ne_{yz} & le_{zz}+m(e_{xx}+e_{yy}) \end{bmatrix}, \tag{9}$$

where

$$m = a_v - b,$$

$$l = a_v + 2b,$$

$$n = \sqrt{3}d, \tag{10}$$

and a_c, a_v, b, d are the usual Pikus-Bir deformation potential constants. The order of k_j relative to the position dependent P_0 and e_{ij} is chosen to be in consistent with Eq. (5). The strain tensor e_{ij} is calculated with the valence force field (VFF) model.[26]

The inclusion of spin-orbit Hamiltonian is straightforward. For the reason of numerical stability as will be shown below, we prefer working with bases

$$|S\uparrow\rangle, |X\uparrow\rangle, |Y\uparrow\rangle, |Z\uparrow\rangle, |S\downarrow\rangle, |X\downarrow\rangle, |Y\downarrow\rangle, |Z\downarrow\rangle. \tag{11}$$

Therefore the spin-orbit Hamiltonian is left undiagonalized and takes the form

$$H_{\mathrm{SO}} = \frac{\Delta}{3}\begin{bmatrix} 0 & 0 & 0 & 0 & 0 & 0 & 0 & 0 \\ 0 & 0 & -i & 0 & 0 & 0 & 0 & 1 \\ 0 & i & 0 & 0 & 0 & 0 & 0 & -i \\ 0 & 0 & 0 & 0 & 0 & -1 & i & 0 \\ 0 & 0 & 0 & 0 & 0 & 0 & 0 & 0 \\ 0 & 0 & 0 & -1 & 0 & 0 & i & 0 \\ 0 & 0 & 0 & -i & 0 & -i & 0 & 0 \\ 0 & 1 & i & 0 & 0 & 0 & 0 & 0 \end{bmatrix}, \quad (12)$$

with Δ the spin split-off energy. The whole eight-band Hamiltonian reads

$$H_8 = \begin{bmatrix} H_4 & 0 \\ 0 & H_4 \end{bmatrix} + \begin{bmatrix} H_{\mathrm{str}} & 0 \\ 0 & H_{\mathrm{str}} \end{bmatrix} + H_{\mathrm{SO}} + V_{\mathrm{conf}}, \quad (13)$$

where V_{conf} accounts for the bandedge discontinuities. The eigenvalue equation to be solved is

$$H_8\mathbf{F} = E\mathbf{F}, \quad (14)$$

where the envelope function $\mathbf{F}$ has eight components

$$[F_{S\uparrow},F_{X\uparrow},F_{Y\uparrow},F_{Z\uparrow},F_{S\downarrow},F_{X\downarrow},F_{Y\downarrow},F_{Z\downarrow}]^T. \quad (15)$$

B. Finite difference scheme

Finite difference (FD) method is widely used to calculate the electronic states of a quantum heterostructure. Since the Hamiltonian is discretized on a real space grid, the inclusion of strain becomes straightforward. However, when one is solving Kane's two-or eight-band model on a collocated grid, i.e., all components of the envelope function are defined on the same grid points, special attention should be payed to the conduction and valence bands coupling terms iPk_i. The commonly used centered difference for the first order spacial derivative is known as unconditionally unstable for the linear hyperbolic equations. We find the similar instability when applying it to Kane's model: spuriously oscillatory solutions arise because even and odd grids are totally decoupled. These spurious solutions were illustrated in Ref. 27 for an InP/InGaAs superlattice. To avoid this numerical instability one can either check the material parameters in the same way as Ref. 27 before using them or choose other FD schemes. In Ref. 13 centered difference is combined with second-order upwind difference to alleviate this problem. The first-order upwind/downwind difference scheme adopted in Ref. 28 for the symmetrized Hamiltonian is another choice and it does not suffer from such instability, however, it is not applicable to the nonsymmetrized Hamiltonian (13) considered here because the geometric symmetry will be broken by this scheme. So in our scheme we perform the discretization on a staggered grid, which is possible by the use of the bases (11). First we discretize F_S (for both spin components) on a cubic grid with an interval Δa (taken to be the lattice constant of GaAs in this work), then we displace this grid in X, Y, Z direction by $\Delta a/2$ on which F_X, F_Y, F_Z are defined, respectively. In this way the centered difference approximation for the first order derivatives is numerically stable so that the spuriously oscillatory solutions will be eliminated. Furthermore it preserves the geometric symmetry of the nonsymmetrized Hamiltonian and is also second order accurate. Note that the different behavior of centered difference on the staggered grid and the collocated grid can be readily verified by a simple Kane's two-band model applied to an GaAs/InAs quantum well, the spuriously oscillatory solutions will appear for the collocated grid, while the staggered grid remains free of such solutions. Also note that the origin of these spurious solutions is purely numerical, different from those discussed in Ref. 22, which are caused by the physical model and are already eliminated in all our calculations as stated in Sec. II A.

C. Eigensolver

After discretization, the Hamiltonian is approximated by a large sparse matrix and what we are interested in are the interior eigenvalues near the conduction and valence band edges. Since the matrix dimension is on the order of 10^6, this interior eigenvalue problem is not a trivial one. Usually a spectral transform technique such as folded spectrum[29] or shift-and-invert method is adopted to change it to a extreme eigenvalue problem, which then is solved by the means of the Lanczos method. In this work we diagonalize the Hamiltonian by the Jacobi-Davidson method,[30] in which the spectral transform can be avoided by the use of Harmonic Ritz values. This greatly reduces the overheads and facilitates this large-scale computation on a single PC. See Ref. 30 for the implementation details. We note that in this method, most efforts are devoted to solving a highly indefinite correction equation with a coefficients matrix $H-\tau I$ projected by some orthogonormal bases, where H is the Hamiltonian matrix, and τ is a target value near the desired eigenvalues. It can be easily shown that if we take Foreman's approach,[22] i.e., set $A_c=0$ to eliminate the physically spurious solutions, then the CB envelopes F_S can be expressed as the linear combinations of F_X, F_Y, F_Z and then be eliminated from the correction equation. Therefore the dimension of the problem is reduced to $\frac{3}{4}$ of the original one. Moreover if we keep the target value τ below the strain modified conduction band edge, then the reduced correction equation becomes a positive definite one, which greatly reduces the computational efforts compared to the original indefinite equation.

III. RESULTS AND DISCUSSION

Before we present the results for the partially capped QD, a brief comparison with Ref. 11 for the fully capped QD is meaningful since we will use the same material parameters as theirs. In addition to the Hamiltonian (symmetrized vs nonsymmetried), the other differences are that we neglect the wetting layer and the piezoelectric effects. The electron and hole ground state energies for a pyramidal QD with the base width equal to 13.6 nm are 1304.8 meV and 168.1 meV, respectively, while these energies are 1274.5 and 176.2 meV in Ref. 11. The discrepancy is reasonable and can be mainly ascribed to the different Hamiltonians used.

In this work we first consider a square-based, truncated pyramidal QD with [110] facets and [001] growth direction.

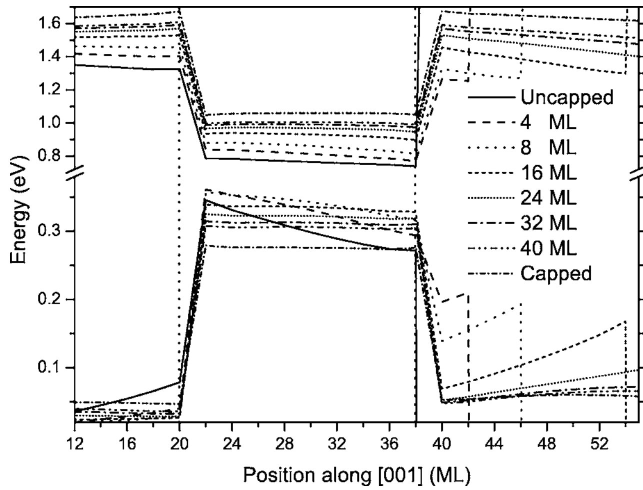

FIG. 2. Strain modified band edges for conduction and valence bands along the principal axis of symmetry of the QD. The left and right vertical dotted lines indicate the position of the QD base and top planes.

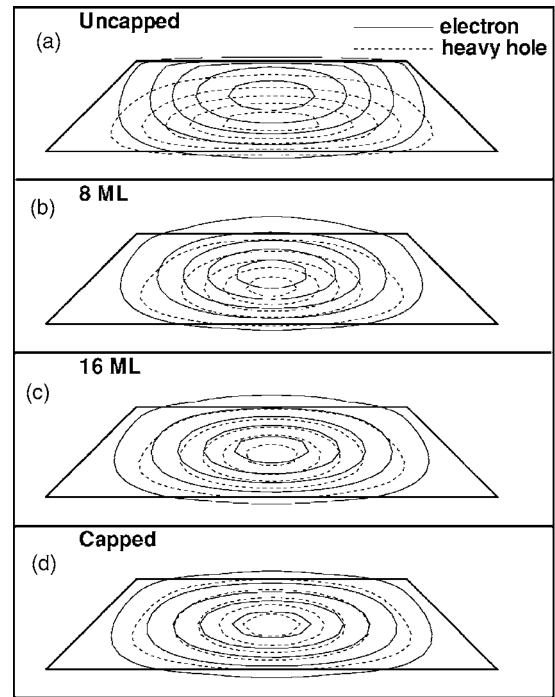

FIG. 3. Contour plots of electron and heavy hole probability density on a [100] cross section through the QD center. (a), (d) are for uncapped and capped cases and (b), (c) for 8 ML and 16 ML thick cap layer. Contour levels are placed at 0.1, 0.3, 0.5, 0.7, 0.9 of its peak value.

The base width and height:width ratio are taken as 25.4 nm and 1:5, respectively. This is the typical size for the QDs experimentally investigated in Ref. 9. In our calculations the GaAs cap layer thickness is assumed to be uniform as shown in the inset of Fig. 1 and the shape change during deposition process is neglected. In this work all the material parameters for GaAs and InAs are taken from Ref. 11 except the deformation potentials, which are taken from Ref. 31.

Figure 1 shows the electron and hole ground state energies and the corresponding dipole transition oscillator strength as a function of the GaAs cap layer thickness. The oscillator strength shown here is for [100]/[010] polarized light. As the cap layer thickness increases, the electron energy increases monotonously from 0.905 (uncapped) to 1.197 eV (capped). This large shift results from large hydrostatic deformation potential a_c (a_c=−5.08 eV for InAs) for the conduction band since the shift amount $\Delta E = a_c e$ where e is the hydrostatic strain. Because the InAs lattice constant is 7% larger than that of GaAs, the QDs will undergo a compressive force at the InAs/GaAs interface. For an uncapped QD, only its bottom interface is under such restriction, while the other 5 InAs/vacuum interfaces (4 [110] facets plus top face) are left with dangling bonds. However, when a GaAs cap layer is deposited, all five interfaces become InAs/GaAs-like and the QD will also experience compressive forces on them. And as the cap layer grows thicker, these forces will become larger. As a result, the edge for the conduction band will be pushed to a higher energy ($a_c < 0$ and $e < 0$ in most of the QD region), which is clearly shown in the upper part of Fig. 2. Here the position along [001] is taken through the QD center. Note that a triangle potential well exists near the QD top face in uncapped and thin cap layer cases. The case of the heavy-hole ground state is more complicated. The energy and band edge do not show a monotonous behavior as the cap layer thickness increases. The small energy shift can only be partly accounted for by the small hydrostatic deformation potential a_v (a_v=1.0 eV for InAs) for the valence band. However, we have to diagonalize a 6×6 matrix containing local strain tensor to obtain the exact local valence band edge. The results for the heavy hole are shown in the lower part of Fig. 2. For uncapped and thin cap layer [<8 monolayers (ML)] cases, the band edge for the heavy hole grows towards higher energy and the base region turns out to be a triangle potential well. When the cap layer becomes thicker (i.e., >8 ML), however, the band edge in the QD region drops in energy and gradually flattens out. As a result, the energy of the heavy hole ground state will first increase from 0.26 (uncapped) to 0.274 eV (8 ML) then decrease to 0.219 eV (capped). Despite this fact the PL peak position will still shows an overall monotonous blueshift because blueshift of electron energy dominates here. Our calculated PL peak positions are 0.645 and 0.978 eV for the uncapped and capped QDs, respectively, which amounts to a 0.333 eV blueshift. We note that the calculated values of PL peak positions are lower in energies than the measured ones reported in Ref. 9. A possible main factor causing such discrepancy between theory and experiment is the strong Ga/In atom interdiffusion during the growth of InAs dots,[32] since the bandgap in the QD region will increase when Ga atoms diffuse into it. However the calculated blueshift agrees very well with the experiment value 306 meV in Ref. 9, so we find that the strain relaxation can fully account for the observed large blueshift in PL. Also note that based on an elastic continuum model, Ref. 9 provides an theoretical estimate of the bandgap change of 194.6 meV, which is smaller than our result. And they attribute the blueshift to the joint influences of the strain relaxation and the confined and surface states couplings, the latter effect is neglected here.

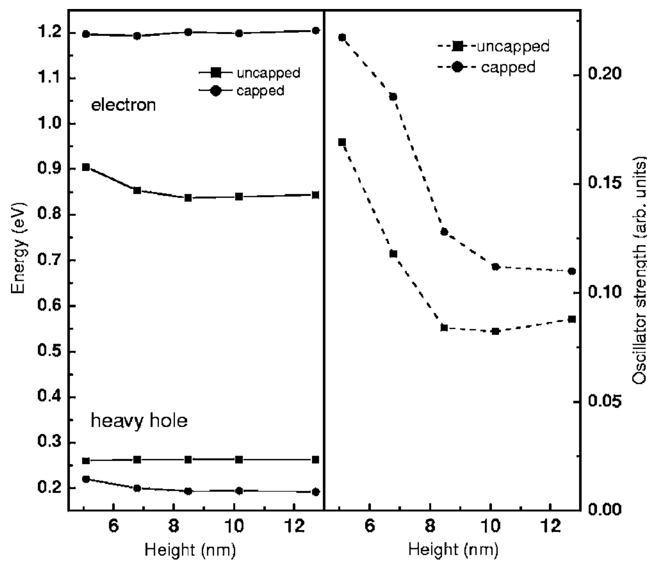

FIG. 4. Ground state energies and oscillator strengths for the [100]/[010] polarized light as a function of QD height. The base width is fixed at 25.4 nm.

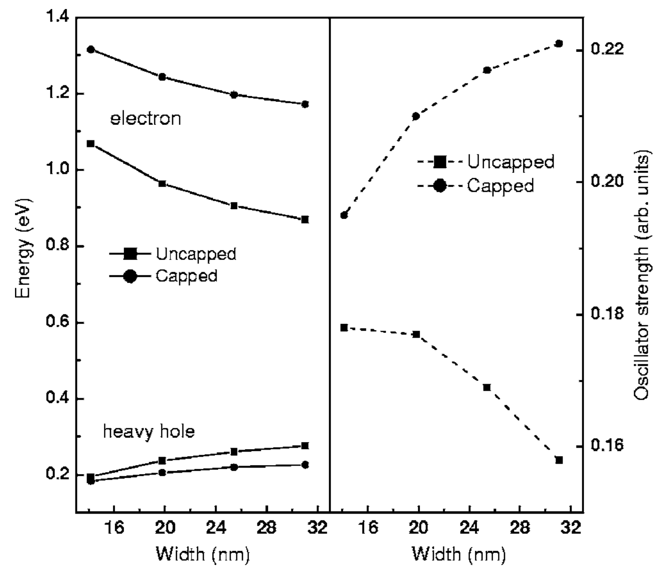

FIG. 5. Ground state energies and oscillator strengths for the [100]/[010] polarized light as a function QD base width. The height:width is fixed at 1:5.

This cap layer induced large blueshift in PL was also reported for InP/InGaP QDs in Ref. 33, where a blueshift of 0.216 eV was observed for a wide thickness range of 0–85 nm. The authors also ascribed the blueshift to the strain modified local bandgap, which was calculated with an elastic model as used in Ref. 9. However, the energy levels for the confined states were not provided, instead, the PL peak was compared with the local bandgap in the center of the QD.

It is well known that the PL intensity is directly proportional to the dipole oscillator strength between the ground states of the electron and heavy hole. In Fig. 1 we can also see that this oscillator strength exhibits a sharp increase as the cap layer grows from 0 to 16 ML and then it saturates till the QD is fully capped. This initial sharp increase was also observed in Ref. 9 where the PL intensity exhibits this behavior from 0 to 7 ML. Our recent experimental results also show that the PL intensity of the capped InGaAs alloy QDs is much stronger than that of the uncapped QDs.[34] As we will show in the following, this phenomenon is a direct consequence of the space separation of the electron and heavy-hole wave functions in the growth direction. In Fig. 3, the contour plots on a [100] cross section through the QD center are given for these squared wavefunctions. As we already noted previously, for the uncapped and thin cap layer cases the top and base regions of the QD are triangle potential wells for electron and heavy hole, respectively. So the peak value for electron/hole wave function will appear near the top/base layer of the QD as shown in Figs. 3(a) and 3(b). Correspondingly, a space separation exists in the growth direction for the electron and heavy hole. However, the separation will gradually diminish as the cap layer grows thicker because the band edges for both conduction and valence bands will flatten out as shown in Fig. 2. Accompanying with the spatial separation diminishing of the electron and heavy-hole wave functions, the oscillator strength and thus PL intensity gradually saturates at 16 ML as shown in Fig. 1, which can be accounted for by Figs. 3(c) and 3(d). The electron and heavy hole wave functions shown in Fig. 3(c) are already very close to those shown in Fig. 3(d). Another possible cause for this PL intensity increase is the suppression of the nonradiative recombination at the surface, as is already pointed out in Ref. 9. However, this effect is beyond our present model.

It should be noted that the above numerical results are strongly dependent on the material parameters used, especially on the deformation potentials since the QDs are highly strained. Unfortunately, large discrepancies exist in the literature for the value of deformation potentials of InAs and GaAs (Refs. 11, 31, and 35–38) and even the sign of a_v remains controversial. Other choices may give quantitatively modification but our qualitative conclusion remains valid.

As can be expected, larger space separation in the growth direction for the electron and heavy hole can be achieved if height:width ratio takes a larger value since more room is available for the electron to move into. To investigate these shape effects, we fix the base width at 25.4 nm and adjust the QD height from 5.1 to 12.7 nm (the corresponding height:width ratio changes from 1:5 to 1:2). For each height value, only two extreme cases are considered: uncapped and fully capped QDs. The results are shown in Fig. 4. The energies do not show a large variation throughout the whole height variation range. The only noticeable energy shift is for the electron of the uncapped QD, where 60 meV redshift occurs when the height changes from 5.1 to 8.5 nm. However, for the oscillator strength, a sharp drop appears in the 5.1 to 8.5 nm range for both capped and uncapped QDs. Further height increase has little influence on the oscillator strength.

Finally we investigate the lateral size influence on the PL properties. The base width is adjusted while the height:width ratio is fixed at 1:5. The result is shown in Fig. 5. As the width increases a redshift of 280 meV occurs for the un-

capped QDs and 186 meV for the cappped QDs due to the quantum confinement effect. As for the oscillator strength, the cap layer thickness has less influence on the smaller QDs. The oscillator strength ratio between the capped and uncapped QDs increases from 1.1 to 1.4 as the base width increases from 14.1 to 31 nm.

IV. CONCLUSIONS

In summary we have performed detailed calculations on the electronic structures of the self-assembled InAs/GaAs QDs. Cap layer thickness turns out to have great influence on the PL peak position and intensity. Strain plays a key role in determining the carriers' ground state energies and spatial distribution, which in turn account for the PL blueshift and intensity increase.

ACKNOWLEDGMENTS

This work was supported by HK RGC-CERG under Contract No. HKU-7049/04P and HKU CRCG funding under Contract No. 10204008 (S.J.X.) and was also supported by a CRCG Grant from HKU (J.W.).

*Author to whom correspondence should be addressed. Electronic address: sjxu@hkucc.hku.hk

[1] D. Bimberg, M. Grundmann, and N. N. Ledentsov, *Quantum Dot Heterostructures* (Wiley, New York, 1998).
[2] N.-T. Yeh, T.-E. Nee, J.-I. Chyi, T. M. Hsu, and C. C. Huang, Appl. Phys. Lett. **76**, 1567 (2000).
[3] F. Ferdos, S. Wang, Y. Wei, A. Larsson, M. Sadeghi, and Q. Zhao, Appl. Phys. Lett. **81**, 1195 (2002).
[4] K. P. Chang, S. L. Yang, D. S. Chuu, R. S. Hsiao, J. F. Chen, L. Wei, J. S. Wang, and J. Y. Chi, J. Appl. Phys. **97**, 083511 (2005).
[5] J. S. Kim, J. H. Lee, S. U. Hong, W. S. Han, H.-S. Kwack, J. H. Kim, and D. K. Oh, J. Appl. Phys. **94**, 2486 (2003).
[6] Z. Y. Zhang, B. Xu, P. Jin, X. Q. Meng, Ch. M. Li, X. L. Ye, and Z. G. Wang, J. Appl. Phys. **92**, 511 (2002).
[7] R. Songmuang, S. Kiravittaya, and O. G. Schmidt, J. Cryst. Growth **249**, 416 (2003).
[8] H. Saito, K. Nishi, and S. Sugou, Appl. Phys. Lett. **73**, 2742 (1998).
[9] Z. L. Miao, Y. W. Zhang, S. J. Chua, Y. H. Chye, P. Chen, and S. Tripathy, Appl. Phys. Lett. **86**, 031914 (2005).
[10] M. Grundmann, O. Stier, and D. Bimberg, Phys. Rev. B **52**, 11969 (1995).
[11] O. Stier, M. Grundmann, and D. Bimberg, Phys. Rev. B **59**, 5688 (1999).
[12] C. Pryor, Phys. Rev. B **57**, 7190 (1998).
[13] H. Jiang and J. Singh, Phys. Rev. B **56**, 4696 (1997).
[14] M. A. Cusack, P. R. Briddon, and M. Jaros, Phys. Rev. B **54**, R2300 (1996).
[15] J. A. Barker and E. P. O'Reilly, Phys. Rev. B **61**, 13840 (2000).
[16] W. Sheng and J.-P. Leburton, Phys. Rev. Lett. **88**, 167401 (2002).
[17] L.-W. Wang, J. Kim, and A. Zunger, Phys. Rev. B **59**, 5678 (1999).
[18] J. Kim, L.-W. Wang, and A. Zunger, Phys. Rev. B **57**, R9408 (1998).
[19] A. J. Williamson and Alex Zunger, Phys. Rev. B **59**, 15819 (1999).
[20] T. Saito, J. N. Schulman, and Y. Arakawa, Phys. Rev. B **57**, 13016 (1998).
[21] R. Santoprete, B. Koiller, R. B. Capaz, P. Kratzer, Q. K. K. Liu, and M. Scheffler, Phys. Rev. B **68**, 235311 (2003).
[22] B. A. Foreman, Phys. Rev. B **56**, R12748 (1997).
[23] M. G. Burt, J. Phys.: Condens. Matter **4**, 6651 (1992).
[24] B. A. Foreman, Phys. Rev. B **48**, R4964 (1993).
[25] T. B. Bahder, Phys. Rev. B **41**, 11992 (1990); **46**, 9913 (1992).
[26] P. Keating, Phys. Rev. **145**, 637 (1966); R. M. Martin, Phys. Rev. B **1**, 4005 (1970).
[27] X. Cartoixà, D. Z.-Y. Ting, and T. C. McGill, J. Appl. Phys. **93**, 3974 (2003).
[28] O. Stier and D. Bimberg, Phys. Rev. B **55**, 7726 (1997).
[29] L.-W. Wang and A. Zunger, J. Chem. Phys. **100**, 2394 (1994).
[30] G. Sleijpen and H. Van der Vorst, SIAM Rev. **42**, 267 (2000).
[31] C. G. Van de Walle, Phys. Rev. B **39**, 1871 (1989).
[32] S. J. Xu, H. Wang, Q. Li, M. H. Xie, W. J. Fan, and S. L. Feng, Appl. Phys. Lett. **77**, 2130 (2000).
[33] M.-E. Pistol, N. Carlsson, C. Persson, W. Seifert, and L. Samuelson, Appl. Phys. Lett. **67**, 1438 (1995).
[34] Z. F. Wei, S. J. Xu, R. F. Duan, Q. Li, J. Wang, and Y. P. Zeng, J. Appl. Phys. **98**, 084305 (2005).
[35] D. D. Nolte, W. Walukiewicz, and E. E. Haller, Phys. Rev. Lett. **59**, 501 (1987).
[36] S.-H. Wei and A. Zunger, Phys. Rev. B **60**, 5404 (1999).
[37] L. W. Wang, A. J. Williamson, A. Zunger, H. Jiang, and J. Singh, Appl. Phys. Lett. **76**, 339 (2000).
[38] R. Santoprete, B. Koiller, R. B. Capaz, P. Kratzer, Q. K. K. Liu, and M. Scheffler, Phys. Rev. B **68**, 235311 (2003).